Electrically responsive structural transformations triggered by vapour and temperature in a series of pleochroic bis(oxalato)chromium(III) complex salts

Marko Dunatov,[a] Andreas Puškarić,[a] Luka Pavić,[a] Zoran Štefanić[a] and Lidija Androš Dubraja*[a]

Stimuli-responsive structural transformations of metal-organic materials are attracting considerable attention due to their potential use in functional switchable devices. In this study, we describe the successful demonstration of a reversible structural transformation triggered by humidity, gaseous methanol, and temperature in a series of complex salts containing bis(oxalato)chromium(III) anions and bicyclic ammonium cations. Synthesis of complex salts with cationic DABCO and ABCO derivatives (DABCO = 1,4-diazabicyclo[2.2.2]octane; ABCO = 1-azabicyclo[2.2.2]octane), and bis(oxalato)chromium(III) $[Cr(bpy)(C_2O_4)_2]^-$ and $[Cr(phen)(C_2O_4)_2]^-$ anions (bpy = 2,2'-bipyridine, phen = 1,10-phenanthroline) was carried out using a green chemistry mechanochemical approach. The salts readily dissolve and can be prepared in the form of single-crystals that show pleochroism when viewed under polarised light, changing their colour from purplish red to orange, similar to the gemstone ruby, which also contains the Cr(III) ions. The characterization of the new complex salts was performed by X-ray diffraction analysis, thermal analysis, infrared spectroscopy and impedance spectroscopy. Interestingly, this series of compounds exhibits reversible single-crystal-to-single-crystal transformations involving dehydration/desolvation and rehydration/resolvation processes. Moreover, these structural transformations are accompanied by significant changes in current response, which makes these compounds interesting for use as sensors and thermistors.

Introduction

Solid-state phase transition compounds with electrically, magnetically, and thermally switchable states generally provide an effective strategy for the design of functional materials such as ferroelectric materials, nonlinear optical switches, sensors and switchable dielectric devices.[1,2] Inorganic-organic hybrid phase transition materials have attracted considerable interest in recent decades due to the prospect of applications in data storage, signal processing, environmental monitoring.[3-5] Among them are the hybrid organic-metal complex salts, usually composed of organic amine cations and inorganic halide anions, which have recently been considered as the most competitive candidates for solar cells.[6] In the field of molecular ferroelectrics, compounds with rotating polar globular ionic molecules, e.g., 1,4-diazabicyclo[2.2.2]octane ($C_6H_{12}N_2$, DABCO) and 1-azabicyclo[2.2.2]octane ($C_7H_{13}N_1$, ABCO), have attracted considerable attention because the realignment of polar molecules can induce ferroelectric polarization in response to an applied electric field.[7-14] Molecule-based dielectrics with dielectric constants in high and low reversible switching states under external factors play an important part in generating switchable dielectric properties owing to their unique combination of structural components.[15] Studying these materials at a molecular level, enables understanding the mechanisms responsible for the stimulus-structure-response property, and potentially leads to construction of better performing and multifunctional devices.[16]

The mononuclear bis(oxalato)chromium(III)complex anions of the general formula $[Cr(NN)(C_2O_4)_2]^-$ (*NN* = α-diimine-type ligand) are well-known supramolecular tectons for the design of heterometallic coordination compounds, and a large number of hetero- as well as homopolynuclear complexes based on these metalloligands have been characterized to date.[17-23] This chemistry has been stimulated primarily by the increasing interest in the search for new molecular-based magnets and the intriguing structural topologies offered by the various coordination modes of the oxalate anion.[24] They are relatively stable species toward substitution reactions and can provide good a priori control over the reaction products.

Here we report the mechanochemically assisted synthesis and characterization of six new complex salts, consisting of bis(oxalato)chromium(III) anions, $[Cr(bpy)(C_2O_4)_2]^-$ and $[Cr(phen)(C_2O_4)_2]^-$ (bpy = 2,2′-bipyridine, phen = 1,10-phenanthroline), and bicyclic ammonium cations, $(H_2\text{-DABCO})^{2+}$, $(CH_3\text{-DABCO})^+$, $(H\text{-OABCO})^+$, $[H\text{-(COOH)(OH)ABCO}]^+$ and $[H\text{-(OH)}_2\text{ABCO}]^+$, shown in Scheme 1. The complex salts $(H_2\text{-DABCO})[Cr(bpy)(C_2O_4)_2]_2\cdot 12H_2O$ (**1**$_{H_2O}$), $(H_2\text{-DABCO})[Cr(phen)(C_2O_4)_2]_2\cdot 9H_2O$ (**2**$_{H_2O}$), $(CH_3\text{-}$

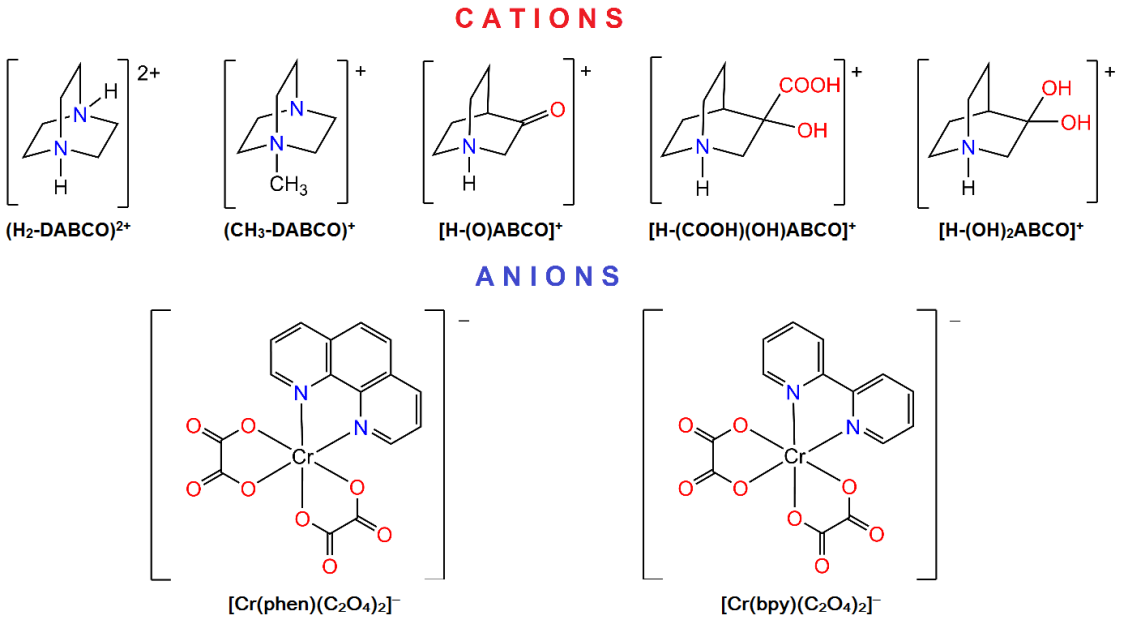

Scheme 1. Organic azabicyclo[2.2.2]octane cations and bis(oxalato)chromium(III) anions used for the synthesis of compounds $\mathbf{1}_{H_2O}$–$\mathbf{6}_{H_2O}$.

DABCO)[Cr(bpy)(C_2O_4)$_2$]·MeOH ($\mathbf{3}_{MeOH}$), [H-(O)ABCO][Cr(bpy)(C_2O_4)$_2$]·H_2O ($\mathbf{4}_{H_2O}$), [H-(COOH)(OH)ABCO][Cr(bpy)(C_2O_4)$_2$]·2H_2O ($\mathbf{5}_{H_2O}$), [H-(OH)$_2$ABCO][Cr(phen)(C_2O_4)$_2$]·2H_2O ($\mathbf{6}_{H_2O}$) were prepared in the form of single-crystals after the mechanochemically obtained product was dissolved and separated from the insoluble precipitate ($BaSO_4$ or AgCl). Crystals show pleochroism, i.e. they change colour from purplish red to orange, depending on the direction of polarization of the light with respect to the crystallographic axes.[25] Another fascinating feature is that crystals of $\mathbf{1}_{H_2O}$, $\mathbf{2}_{H_2O}$ and $\mathbf{3}_{MeOH}$ undergo a reversible single-crystal-to-single-crystal transformation to the desolvated phases (H_2-DABCO)[Cr(bpy)(C_2O_4)$_2$]$_2$ (**1**), (H_2-DABCO)[Cr(phen)(C_2O_4)$_2$]$_2$ (**2**) and (CH_3-DABCO)[Cr(bpy)(C_2O_4)$_2$] (**3**) when dried in air. The rehydration can be achieved when the crystals of **1**–**3** are exposed to humid air or, in case of compound **3**, exposure to methanol vapour gives $\mathbf{3}_{MeOH}$. Characterization of the new complex salts was performed by single-crystal and powder X-ray diffraction analysis, thermal analysis, attenuated total reflectance infrared spectroscopy, diffuse reflectance UV-Vis spectroscopy and impedance spectroscopy. Moreover, there is a noticeable correlation between the structural changes during desolvation/resolvation and the conductivity of these systems, which was determined by chronoamperometric measurements.

Experimental

Measurements

The attenuated total reflection (ATR) spectra were recorded in the 4000–400 cm^{-1} region with a Perkin–Elmer FT-IR Frontier spectrometer. Diffuse reflectance UV-Vis spectra were obtained on a Shimadzu UV-Vis-NIR spectrometer (model UV-3600) equipped with an integrated sphere. The diffuse reflectance spectra were transformed using the Kubelka–Munk function. Thermal analysis was performed with a Shimadzu DTG-60H analyser, in the range from room temperature to 1073 K, in a stream of synthetic air at a heating rate of 10 K min^{-1}. NMR spectra were recorded on 300 MHz spectrometers, operating at 75.47 MHz for ^{13}C and 300.13 MHz for ^{1}H nuclei. TMS was used as an internal standard. The dielectric properties were studied by impedance spectroscopy using an impedance analyser (Novocontrol Alpha-N dielectric spectrometer) at room temperature in the frequency range from 0.1 Hz to 1 MHz. Also, measurements were made in isofrequency mode at 10 and 100 kHz on heating from 183 to 363–423 K and subsequently cooling down to 183 K. For these measurements a polycrystalline sample was pressed into a cylindrical pellet of thickness ~0.75 mm and placed between brass electrodes which served as electrical contacts. Current response of compounds **1**, **2** and **3** pressed into a cylindrical pellet of thickness ~0.2 mm was monitored during the desolvation/resolvation process with PalmSens4 potentiostat. Chamber was constructed having a manual device for adjustment and monitoring the relative humidity (RH). A certain amount of dry or wet gas was used to decrease or increase the interior humidity of device. Thermistor properties of single-crystal $\mathbf{4}_{H_2O}$ have been tested on a Keithley Model 6487 picoammeter/voltage source during rapid change

in heating and cooling cycles. Electrical contacts were made with silver paste.

Synthetic procedures

1,4-diazabicyclo[2.2.2]octane (DABCO) and 1-azabicyclo[2.2.2]octan-3-one hydrochloride [H-(O)ABCO]Cl were purchased from Alfa Aesar. The $[Ba(H_2O)Cr_2(bpy)_2(C_2O_4)_4]_n{\cdot}nH_2O$ and $[Ba(H_2O)_2Cr_2(phen)_2(C_2O_4)_4]_n{\cdot}2nH_2O$ were prepared following the reported procedure for $[SrCr_2(bpy/phen)_2(C_2O_4)_4]{\cdot}nH_2O$ but using $Ba(NO_3)_2$ instead of $Sr(NO_3)_2$.[23] $[Ag(H_2O)_2Cr(bpy)(C_2O_4)_2]_2$ and $[Ag(H_2O)_2Cr(phen)(C_2O_4)_2]_2$ were prepared from the reaction of Ag_2SO_4 and $[Ba(H_2O)Cr_2(bpy)_2(C_2O_4)_4]_n{\cdot}nH_2O$ and $[Ba(H_2O)_2Cr_2(phen)_2(C_2O_4)_4]_n{\cdot}2nH_2O$, respectively. Mechanochemical synthesis were performed with Retsch MM 400 mixer mill at a frequency of 25 Hz, in the 4 mL poly(methyl methacrylate) grinding jars using one 7 mm stainless steel ball.

Synthesis of 1,4-diazoniabicyclo[2.2.2]octane sulphate, (H_2-DABCO)SO_4. DABCO (0.11 g, 1 mmol) was dissolved in 1M aqueous solution of H_2SO_4 (1 mL). White crystals of (H_2-DABCO)SO_4 formed after evaporation in quantitative yield.

Synthesis of 1-methyl-4-aza-1-azoniabicyclo[2.2.2]octane sulphate, (CH_3-DABCO)$_2SO_4$. 1-methyl-4-aza-1-azoniabicyclo[2.2.2]octane iodide was prepared following reported procedure from the reaction of DABCO and CH_3I in ethyl acetate.[26] It was converted to (CH_3-DABCO)$_2SO_4$, by reaction of (CH_3-DABCO)I with Ag_2SO_4 in aqueous solution (2 : 1). ^{1}H NMR (600 MHz, DMSO): δ (ppm) 3.27 (m, 6H), 3.02 (m, 6H), 2.97 (s, 3H); ^{13}C NMR (150 MHz, DMSO): δ (ppm) 53.3, 50.8, 44.7.

Synthesis of 3-Hydroxy-1-azabicyclo[2.2.2]octane-3-carboxylic acid hydrochloride [H-(COOH)(OH)ABCO]Cl. [H-(COOH)(OH)ABCO]Cl was prepared following reported procedure.[27] To an ice-cold solution of [H-(O)ABCO]Cl (1.6 g, 10 mmol) in 5 ml of water, a solution of KCN (0.65 g, 10 mmol) in 5 ml of water was added dropwise. Reaction mixture was stirred for a further hour in ice bath, and then 3-hydroxy-3-cyano-1-azabicyclo[2.2.2]octane was filtered off and washed out with a little ice water. The yield was 1,2 g (78%). 3-hydroxy-3-cyano-1-azabicyclo[2.2.2]octane (0.80 g, 5 mmol) was dissolved in 12 mL of concentrated HCl and left to stand at 293 K for 48 hours. White solid of [H-(COOH)(OH)ABCO]Cl was separated from the solution by filtration and washed with diethyl-ether. The yield was 0.606 g (56%). ^{1}H NMR (600 MHz, D_2O): δ (ppm) 3.96 (d, J = 2.3 Hz, 1H), 3.93 (d, J = 2.3 Hz, 1H), 3.32–3.17 (m, 2H), 3.14 (d, J = 2.0 Hz, 1H), 3.12 (d, J = 2.1 Hz 1H), 2.35 (quint, J = 3.1 Hz 1H), 2.29–2.21 (m, 1H), 1.98–1.89 (m, 1H), 1.88–1.78 (m, 2H); ^{13}C NMR (150 MHz, D_2O): δ (ppm) 175.4, 72.6, 55.9, 46.1, 45.5, 28.7, 18.9, 17.0.

Synthesis of (H_2-DABCO)$[Cr(bpy)(C_2O_4)_2]_2{\cdot}12H_2O$ ($\mathbf{1}_{H_2O}$) and (H_2-DABCO)$[Cr(bpy)(C_2O_4)_2]_2$ (1). (H_2-DABCO)SO_4 (11 mg; 0.05 mmol) and $[Ba(H_2O)Cr_2(bpy)_2(C_2O_4)_4]_n{\cdot}nH_2O$ (47 mg; 0.05 mmol) were mixed and milled for 60 minutes. Then 10 mL of water was added to reaction mixture and a white precipitate ($BaSO_4$) was removed by filtration. From the resulting clear red solution, purplish red/orange needle-like crystals of $\mathbf{1}_{H_2O}$ crystallized by slow evaporation. The yield was 33 mg (60%). ATR, cm^{-1}: 3420 (m, br), 1705 (s), 1670 (vs), 1652 (vs), 1603 (s), 1474 (m), 1448 (m), 1365 (vs), 1317 (m), 1248 (m), 1160 (m), 1059 (m), 1035 (m), 1023 (m), 893 (m), 796 (vs), 768 (s), 732 (m), 544 (vs). When crystals of $\mathbf{1}_{H_2O}$ are left to dry in air at room temperature, transformation to crystals of **1** is observed.

Synthesis of (H_2-DABCO)$[Cr(phen)(C_2O_4)_2]_2{\cdot}9H_2O$ ($\mathbf{2}_{H_2O}$) and (H_2-DABCO)$[Cr(phen)(C_2O_4)_2]_2$ (2). (H_2-DABCO)SO_4 (11 mg; 0.05 mmol) and $[Ba(H_2O)_2Cr_2(phen)_2(C_2O_4)_4]_n{\cdot}2nH_2O$ (50 mg; 0.05 mmol) were mixed and milled for 60 minutes. Then 10 mL of water was added to reaction mixture and a white precipitate ($BaSO_4$) was removed by filtration. From the resulting clear red solution, purplish red/orange plate-like crystals of $\mathbf{2}_{H_2O}$ crystallized by slow evaporation. The yield was 16 mg (30%). ATR, cm^{-1}: 3407 (m, br), 1703 (s), 1676 (vs), 1608 (s), 1585 (m), 1520 (m), 1427 (m), 1367 (s), 1224 (m), 854 (m), 801 (s), 741 (w), 722 (s), 547 (s). When crystals of $\mathbf{2}_{H_2O}$ are left to dry in air at room temperature, transformation to crystals of **2** is observed.

Synthesis of (CH_3-DABCO)$[Cr(bpy)(C_2O_4)_2]{\cdot}MeOH$ ($\mathbf{3}_{MeOH}$), (CH_3-DABCO)$[Cr(bpy)(C_2O_4)_2]{\cdot}$(3) and ($CH_3$-DABCO)$[Cr(bpy)(C_2O_4)_2]{\cdot}5H_2O$ ($\mathbf{3}_{H_2O}$). (CH_3-DABCO)$_2SO_4$ (18 mg, 0.05 mmol) and $[Ba(H_2O)Cr_2(bpy)_2(C_2O_4)_4]_n{\cdot}nH_2O$ (57 mg, 0.05 mmol) were mixed and milled for 60 minutes. Then 10 mL of 1:1 MeOH/MeCN was added to reaction mixture and a white precipitate ($BaSO_4$) was removed by filtration. From the resulting clear red solution, purplish red/orange prism-like crystals of $\mathbf{3}_{MeOH}$ were isolated after 48 h of standing at 276 K. The yield was 33 mg (60%). ATR, cm^{-1}: 3675 (w), 3423 (w), 3081 (m), 1704 (s), 1675 (vs), 1609 (s), 1601 (s), 1471 (m), 1441 (m), 1350 (s), 1321 (s), 1286 (m), 1238 (m), 1215 (s), 1156 (m), 1058 (m), 1035 (m), 1023 (m), 881 (m), 844 (m), 793 (vs), 781 (s), 734 (m), 542 (m), 452 (m). When crystals of $\mathbf{3}_{MeOH}$ are left to dry in air at room temperature, transformation to crystals of **3** is observed. Crystals of **3** can be converted to the hydrated form $\mathbf{3}_{H_2O}$ if exposed to air with RH > 90%.

Synthesis of [H-(O)ABCO]$[Cr(bpy)(C_2O_4)_2]{\cdot}H_2O$ ($\mathbf{4}_{H_2O}$). [H-(O)ABCO]Cl (16 mg, 0.1 mmol) was mixed with $[Ag(H_2O)_2Cr(bpy)(C_2O_4)_2]_2$ (53 mg, 0.05 mmol) and milled for 60 minutes. Then 10 mL of water was added to reaction mixture and a white precipitate (AgCl) was removed by filtration. From the resulting clear red solution, red plate-like crystals of $\mathbf{4}_{H_2O}$ crystallized after the solvent had almost evaporated. The yield was 32 mg (60%). ATR, cm^{-1}: 3567 (w), 3492 (w), 3123 (w), 1743 (m), 1709 (s), 1690 (s), 1671 (vs), 1624 (s), 1603 (m), 1445 (m), 1392 (s), 1369 (vs), 1318 (m), 1237 (s), 1074 (m), 1037 (m), 894 (m), 790 (s), 778 (s), 734 (m), 651 (m), 544 (s), 451 (m), 407 (vs).

Synthesis of [H-(COOH)(OH)ABCO]$[Cr(bpy)(C_2O_4)_2]{\cdot}2H_2O$ ($\mathbf{5}_{H_2O}$). [H-(COOH)(OH)ABCO]Cl (20 mg, 0.1 mmol) was mixed with $[Ag(H_2O)_2Cr(bpy)(C_2O_4)_2]_2$ (53 mg, 0.05 mmol) and milled for 60 minutes. Then 10 mL of water was added to reaction mixture and a white precipitate (AgCl) was removed by filtration. From the resulting clear purplish red solution, purplish red/orange plate-like crystals of $\mathbf{5}_{H_2O}$ appeared after 72 h of standing at 276 K. The yield was 36 mg (60%). ATR, cm^{-1}: 3356 (w, br), 1712 (s), 1703 (s), 1661 (vs), 1611 (m), 1602 (s), 1446 (m), 1364 (vs), 1317 (m), 1248 (m), 1215 (m), 1190 (m), 1140 (m), 1104 (w), 1088 (w), 1064 (m), 887 (m), 797 (s), 769 (vs), 734 (m), 646 (m), 546 (s), 453 (m).

Synthesis of [H-(OH)$_2$ABCO][Cr(phen)(C$_2$O$_4$)$_2$]·2H$_2$O (6$_{H_2O}$). [H-(O)ABCO]Cl (16 mg, 0.1 mmol) was mixed with [Ag(H$_2$O)Cr(phen)(C$_2$O$_4$)$_2$]$_2$ (55 mg, 0.05 mmol) and milled for 60 minutes. Then 10 mL of water was added to reaction mixture and a white precipitate (AgCl) was removed by filtration. From the resulting clear purplish red solution, purplish red/orange plate-like crystals of **6$_{H_2O}$** appeared after the solvent had almost evaporated. The yield was 35 mg (60%). ATR, cm^{-1}: 3514 (m), 3415 (m, br), 3064 (m), 1702 (s), 1678 (vs), 1661 (vs), 1585 (m), 1521 (m), 1428 (m), 1400 (m), 1372 (s), 1318 (m), 1251 (m), 1239 (m), 1214 (m), 1138 (m), 1086 (m), 1013 (m), 947 (m), 877 (m), 858 (m), 800 (s), 741 (m), 722 (s), 656 (m), 547 (s).

Crystallography

The X-ray diffraction data for single crystals were collected by *ω*-scans using Cu-Kα radiation (λ = 1.54179 Å, microfocus tube, mirror monochromator) on an Oxford Diffraction Xcalibur Nova R diffractometer at room temperature (293 K) for **1**, **2$_{H_2O}$**, **3**, **4$_{H_2O}$**, **5$_{H_2O}$** and **6$_{H_2O}$**, and on a Rigaku XtaLAB Synergy diffractometer at 140 K for **1$_{H_2O}$**, 220 K for **3$_{MeOH}$**, and 400 K for **4**. Data reduction, including the multiscan absorption correction, was performed with the CrysAlisPRO software[28] package. The crystal data, experimental conditions and final refinement parameters are summarized in Table S1 in ESI†. Molecular and crystal structures were solved by direct methods using the program SIR2019,[29] and refined by the full-matrix least-squares method based on F^2 with anisotropic displacement parameters for all non-hydrogen atoms (SHELXL-2014/7).[30] Both programs were operating under the WinGX[31] program package. Three water molecules (O23, O24 and O25) and six carbon atoms (C33–C38) of (H$_2$-DABCO)$^{2+}$in **2$_{H2O}$**, oxygen atom of MeOH in **3$_{MeOH}$**, and oxygen atom of [H-(O)ABCO]$^+$ in **4** are disordered in two positions and their site occupancies were refined. Hydrogen atoms attached to the C atoms of the bpy and phen ligands as well as (H$_2$-DABCO)$^{2+}$, (CH$_3$-DABCO)$^+$, [H-(O)ABCO]$^+$, [H-(COOH)(OH)ABCO]$^+$ and [H-(OH)$_2$ABCO]$^+$ cations were treated as riding in idealized positions, with the C–H distances of 0.93 Å and displacement parameters assigned as U_{iso}(H) = 1.2U_{eq}(C). Hydrogen atoms for disordered water molecules in compound **2$_{H_2O}$** were not determined. Other hydrogen atoms were identified based on difference Fourier maps [O–H distances were restrained to a target value of 0.85(2) Å, and the H–O–H angle to 104°]. Geometrical and solvent accessible voids calculations were carried out with the program PLATON[32]. Figures were generated using the CCDC-Mercury program.[33]

The X-ray powder diffraction data (XRPD) were collected in reflection mode with Cu-Kα radiation (λ = 1.54060 Å) on a Malvern Panalytical Empyrean diffractometer using a step size of 0.001° in the 2θ range between 5° and 50°. Peak search and indexing for compounds **1** and **3$_{H_2O}$** were carried out using the TOPAS software.[34] Unit cell and profile refinement were carried out using the Pawley method.[35] XRPD pattern and profile fitting results are given in ESI†, Figure S1–S6 and Table S2.

Results and discussion

Synthesis and spectroscopic characterization

The complex salts **1$_{H_2O}$**, **2$_{H_2O}$** and **3$_{MeOH}$** were prepared using a straightforward approach based on the replacement of the Ba(II) cations from the coordination polymers [Ba(H$_2$O)Cr$_2$(bpy)$_2$(C$_2$O$_4$)$_4$]$_n$·nH$_2$O[18] and [Ba(H$_2$O)$_2$Cr$_2$(phen)$_2$(C$_2$O$_4$)$_4$]$_n$·2nH$_2$O[19] with derivatives of DABCO- and ABCO-based cations in the form of sulphates. Due to the low solubility of these coordination polymers, the cation substitution reactions were carried out mechanochemically. Complex salts **4$_{H_2O}$**–**6$_{H_2O}$** were synthesised by the same strategy but using Ag(H$_2$O)$_2$Cr(bpy)(C$_2$O$_4$)$_2$]$_2$[20] and [Ag(H$_2$O)$_2$Cr(phen)(C$_2$O$_4$)$_2$]$_2$ and DABCO- and ABCO-based cations in the form of chlorides. In the synthesis of compound **6$_{H_2O}$**, the addition of water to [H-(O)ABCO]$^+$ cation is apparently catalysed by the precursor [Ag(H$_2$O)$_2$Cr(phen)(C$_2$O$_4$)$_2$]$_2$, resulting in a geminal diol [H-(OH)$_2$ABCO]$^+$ cation. The newly formed complex salts are readily dissolved in a water or MeOH/MeCN solution, separated from the insoluble BaSO$_4$/AgCl, and subsequently grown as large single-crystals. Compounds **1$_{H_2O}$**–**6$_{H_2O}$** can also be prepared directly from solution, but in much lower yields limited by the solubility of the Ba(II) and Ag(I) bis(oxalate)chromium(III) precursors. An interesting optical phenomenon, pleochroism, is observed in crystals of **1$_{H_2O}$**, **2$_{H_2O}$**, **3$_{MeOH}$**, **5$_{H_2O}$** and **6$_{H_2O}$**. When polarised light passes through the crystals, it is absorbed differently in different directions, and these crystals appear orange or purplish red (Figure 1 and Figure S7). This property is the result of crystal anisotropy and the required balance between energy, intensity, and anisotropy of light absorptions allowed by crystal symmetry.[19] There are only few examples of pleochroic metal-organic crystals, making this phenomenon special and much less studied compared to other optical properties.[25,36,37]

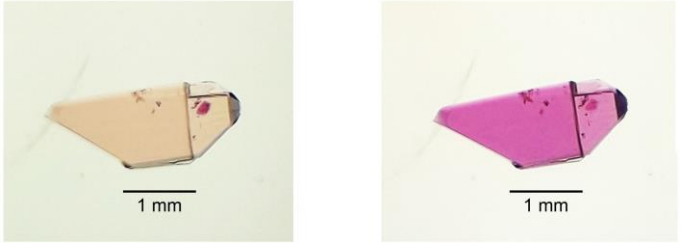

Figure 1. Photograph of a (H$_2$-DABCO)[Cr(phen)(C$_2$O$_4$)$_2$]$_2$·9H$_2$O (**2$_{H_2O}$**) single-crystal changing colour from orange to purplish red when the polariser was rotated for 90°.

The optical properties of single crystal of compound **3$_{MeOH}$** were analysed by UV–vis diffuse reflectance spectroscopy. Kubelka–Munk diffuse reflectance absorption spectra are presented in **Figure 2**. Absorption spectra of crystals reveal the origin of differences in colour with respect to different orientation of the crystal. Absorption in the range 400–480 nm is larger for orange crystals. When crystals are rotated by 90° an absorption peak at 585 nm appears, giving the purple colour of the crystals. In addition to single crystal measurements we recorded the UV-visible diffuse reflectance spectrum of the grinded (powder) sample. This spectrum is exhibiting splitting of the d–d spin-allowed transitions, typical for a distorted octahedral geometry of chromium(III).[38] The lowest $^4T_{2g}$←$^4A_{2g}$

transition is split into $^4E_g \leftarrow {}^4B_{1g}$ and $^4B_{2g} \leftarrow {}^4B_{1g}$, and the corresponding bands are located at 535 and 445 nm, respectively. Similarly, the second spin-allowed transition $^4T_{1g} \leftarrow {}^4A_{2g}$ is also split, appearing at 399 and 416 nm.[21–23]

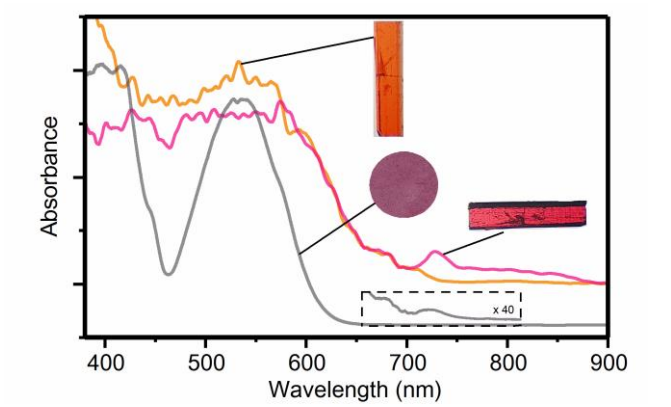

Figure 2. Solid-state UV-visible diffuse reflectance spectra of compound $\mathbf{3_{MeOH}}$ measured on a single crystal oriented in different directions (0 and 90 ° rotation) and in the powder form, and the corresponding images of crystals and powder.

ATR spectroscopy was used to follow the crystal transformation of solvated forms $\mathbf{1_{H_2O}}$–$\mathbf{3_{H_2O}}$, and $\mathbf{3_{MeOH}}$ into solvent-free forms **1**, **2**, and **3**, respectively. The ATR spectra (Figures S8–S13) of the complex salts $\mathbf{1_{H_2O}}$–$\mathbf{6_{H_2O}}$ and $\mathbf{3_{MeOH}}$ contain a broad band between 3600 and 3300 cm^{-1}, assigned to O–H stretching vibrations of the solvent molecules (water and methanol). These bands are not present in the desolvated forms **1**, **2** and **3**. Moreover, the very strong bands between 1660 and 1680 cm^{-1}, originating from asymmetric C–O stretching vibrations in oxalate anions,[21–23] change upon desolvation/resolvation, which can be seen in Figures S8–S13 in ESI†. The positions and intensities of these bands change slightly due to the newly formed hydrogen bonds between oxalate groups of the $[Cr(bpy/phen)(C_2O_4)_2]^-$ anions and solvent molecules in the solvated forms $\mathbf{1_{H_2O}}$–$\mathbf{3_{H_2O}}$ and $\mathbf{3_{MeOH}}$. Furthermore, the strong band at 1712 cm^{-1} in the spectrum of compound $\mathbf{5_{H_2O}}$ is characteristic of the C=O stretching of the carboxylic acid. Also, the spectrum of compound $\mathbf{4_{H_2O}}$, shows a band at 1709 cm^{-1} characteristic of the C=O stretching of the ketone.[39] The absence of the vibration characteristic of the ketone group in the spectrum of compound $\mathbf{6_{H_2O}}$ indicates that reduction of the carbonyl group has occurred.

Crystal structures

Compounds $\mathbf{1_{H_2O}}$ and $\mathbf{2_{H_2O}}$ crystallize in the triclinic space group $P\bar{1}$, while $\mathbf{3_{MeOH}}$, $\mathbf{4_{H_2O}}$, and $\mathbf{6_{H_2O}}$ have a monoclinic $P2_1/c$ structure. The highest symmetry in this series of compounds is exhibited by compound $\mathbf{5_{H_2O}}$ with an $[H\text{-}(COOH)(OH)ABCO]^+$ cation, which gives the orthorhombic *Pbca* structure. The chromium environment is essentially the same in all prepared compounds: a distorted octahedron consisting of four oxygen atoms originating from two oxalate groups and two nitrogen atoms originating from bpy or phen molecule. The Cr–O bond distances are between 1.947(1) and 1.970(2) Å and the Cr–N bond distances are between 2.058(2) and 2.080(2) Å. The angles involving the two oxalates at the chromium atom are in the range of 82.42(8)–83.27(8)°, while the N–Cr–N angles are in the range of 78.31(9)–80.16(6)°.[18–23] Asymmetric units with cations and anions are shown in Figure 3 for compounds $\mathbf{1_{H_2O}}$, $\mathbf{2_{H_2O}}$, $\mathbf{3_{MeOH}}$, and $\mathbf{4_{H_2O}}$, and in Figure 4 for compounds $\mathbf{5_{H_2O}}$ and $\mathbf{6_{H_2O}}$. Compounds $\mathbf{1_{H_2O}}$ and $\mathbf{2_{H_2O}}$ have a layered structure consisting of a hydrophobic part, in which the bpy/phen molecules of bis(oxalato)chromium(III) anions form aromatic stacks, and a hydrophilic part, in which the water molecules of crystallization surround the $(H_2\text{-}DABCO)^{2+}$ cations. In compound $\mathbf{3_{MeOH}}$ the crystal packing consists of discrete aromatic stacks between bpy molecules, and hydrogen bonds between methanol and the oxalate ligand of the $[Cr(bpy)(C_2O_4)_2]^-$ anion. In compounds $\mathbf{4_{H_2O}}$–$\mathbf{6_{H_2O}}$, the organic cations and the mononuclear anions are linked by an (ABCO)N–H ···O(oxalate) hydrogen bond in addition to the electrostatic interaction. Compounds $\mathbf{5_{H_2O}}$ and $\mathbf{6_{H_2O}}$ with additional donor atoms on the organic cations (-OH and -COOH groups) form an extensive hydrogen bonding network. Aromatic interactions are also present: in $\mathbf{4_{H_2O}}$ and $\mathbf{5_{H_2O}}$ the aryl rings of the $[Cr(bpy)(C_2O_4)_2]^-$ anions form discrete stacks; while in $\mathbf{6_{H_2O}}$ an extended stacking interaction between the aryl rings of the $[Cr(phen)(C_2O_4)_2]^-$ anions is observed, along the *c*-axis.

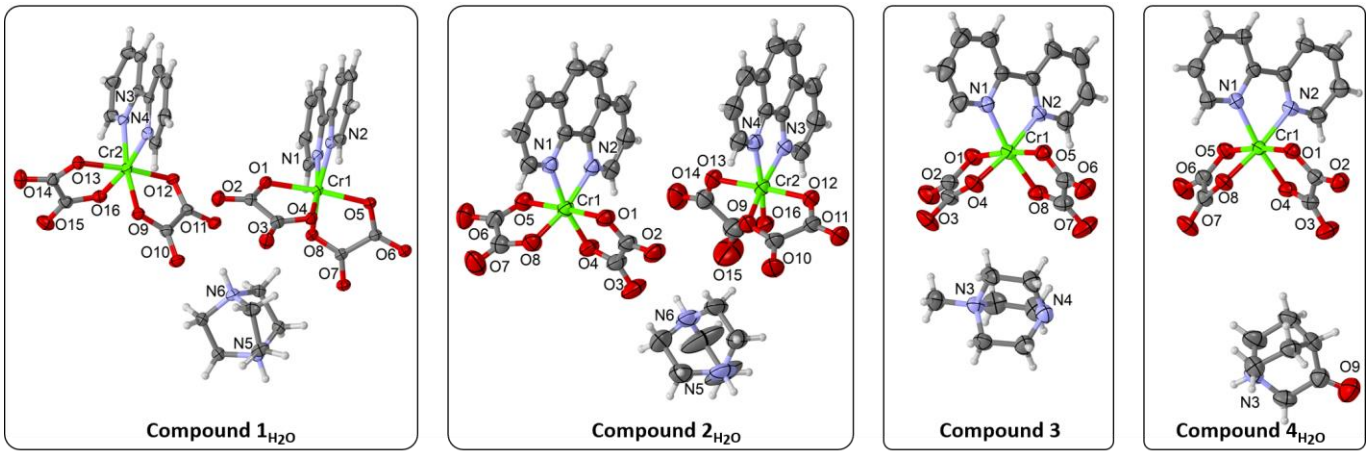

Figure 3. Asymmetric unit of $\mathbf{1_{H_2O}}$, $\mathbf{2_{H_2O}}$, **3**, and $\mathbf{4_{H_2O}}$ showing non-hydrogen atoms as ellipsoids with 50% probability and hydrogens as spheres of arbitrary radii, with labels for all non C, H atoms. Solvent molecules have been omitted for clarity.

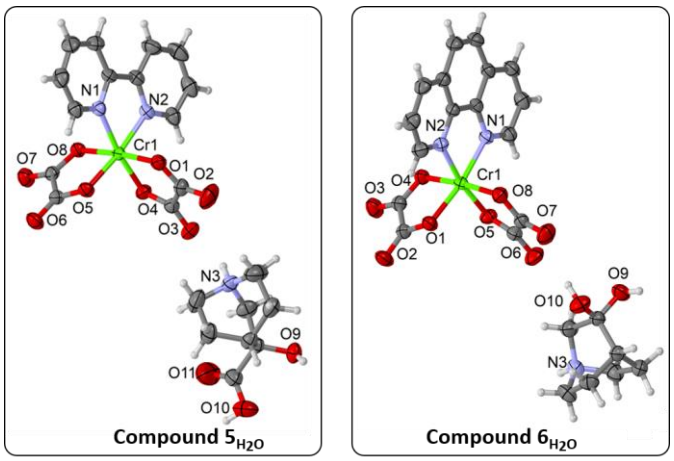

Figure 4. Asymmetric unit of $\mathbf{5}_{H_2O}$ and $\mathbf{6}_{H_2O}$ showing non-hydrogen atoms as ellipsoids with 50% probability and hydrogens as spheres of arbitrary radii, with labels for all non C, H atoms. Solvent molecules have been omitted for clarity.

Structural transformations

Reversible structural transformations dependent on environmental conditions (humidity, alcohol vapours, and temperature) that occur in compounds **1–4** are simplified in Scheme 2. When a single-crystal of $\mathbf{1}_{H_2O}$ is removed from the mother liquid and allowed to air dry, it transforms into a solvent-released form **1** (XRPD patterns in Figure S3). The simultaneous loss of twelve water molecules from the crystal results in a change in space group, changing from $P\bar{1}$ to $P2_1/c$, and the total volume of the unit cell is reduced by 23% (539 Å^3). Compound **1** consists only of $[Cr(bpy)(C_2O_4)_2]^-$ complex anions and $(H_2\text{-DABCO})^{2+}$ cations. As can be seen in Figure 5a, there is an off-set-face-to-face aromatic stacking interaction between the aryl rings of the $[Cr(bpy)(C_2O_4)_2]^-$ complex anions running along the *c*-axis in $\mathbf{1}_{H_2O}$ and **1**. Removal of lattice water molecules causes the $[Cr(bpy)(C_2O_4)_2]^-$ complex anions to rotate in the opposite direction, and take positions according to the introduced *c*-glide plane in a dehydrated form **1** with higher symmetry. A similar process of crystal transformation is observed for compound $\mathbf{2}_{H_2O}$, leading to the formation of dehydrated from **2** (Figure S4). Interestingly, compound **3** shows multiple and reversible single-crystal-to-single-crystal transformations when exposed to air, humid air (RH > 90%) or methanol vapour (Figure 5b). The initially obtained phase $\mathbf{3}_{MeOH}$ with methanol as a crystallization solvent molecule is converted to a desolvated form **3** after removal from the mother liquid. The desolvation process is accompanied by the loss of symmetry from monoclinic $P2_1/c$ to triclinic $P\bar{1}$. When compound **3** is exposed to methanol vapour, it converts back to the initial $\mathbf{3}_{MeOH}$ phase, as detected by the XRPD and ATR measurements (Figure S5). Another prominent feature of compound **3** is its ability to accommodate water molecules when exposed to air with high relative humidity (RH > 90%), and it converts to a new phase $\mathbf{3}_{H_2O}$ (Figure S5) having a monoclinic $P2_1/a$ structure. The ability to accommodate a large number of guest (solvent) molecules is very common in microporous metal-organic frameworks due to structural features such as interstitial channels and large cavities.[40-42] Structural transformation involving hydrated and dehydrated forms have been recently reported in a one dimensional coordination compound $Cs[MnCl_3(H_2O)_2]$. In this system structural transformations induced by loss of two water molecules are accompanied by a change in luminescent properties.[43] For complex salts **1**-**3**, without coordination networks and free solvent-accessible volume, it was indeed unexpected to observe such breathable property of the crystal structure. According to analyses of solvent accessible voids calculated by Platon[32] water molecules are occupying 30% of the total unit cell volume in compound $\mathbf{1}_{H_2O}$, resembling to protein crystals which contain a significant fraction of water. The process of removal and uptake of MeOH is completely reversible for the $\mathbf{3}\leftrightarrow\mathbf{3}_{MeOH}$ system, and this is also observed for the dehydration and hydration process in $\mathbf{1}\leftrightarrow\mathbf{1}_{H_2O}$, $\mathbf{2}\leftrightarrow\mathbf{2}_{H_2O}$ and $\mathbf{3}\leftrightarrow\mathbf{3}_{H_2O}$ systems. To gain insight into the dynamics of structural transitions in the $\mathbf{1}\leftrightarrow\mathbf{1}_{H_2O}$ and $\mathbf{3}_{MeOH}\leftrightarrow\mathbf{3}\leftrightarrow\mathbf{3}_{H_2O}$ systems, *in situ* ATR measurements were performed in dry air atmosphere (RH < 30%), humid air atmosphere (RH > 90%), and dry air atmosphere saturated with MeOH vapour (Figures S14 and S15 in the ESI). These experiments show that the process of water removal from the wet phase $\mathbf{1}_{H_2O}$ starts immediately after exposure to dry air and after 7 minutes only the dry phase **1** exists. Recovery of the wet phase is complete after exposure to humid air for 10 minutes. Complete loss of the methanol molecule from $\mathbf{3}_{MeOH}$ occurs after 25 minutes of exposure to dry air, resulting in phase **3**. The original $\mathbf{3}_{MeOH}$ phase is restored after a 5-minute exposure to dry air saturated with MeOH vapour. In the humid atmosphere, phase **3** is converted to $\mathbf{3}_{H_2O}$ after 18 minutes and returned to phase **3** after 12 minutes in dry air.

Compound $\mathbf{4}_{H_2O}$ undergoes a thermally induced reversible phase transition at 378 K (Figure S6), which is accompanied by the loss of the water molecule of crystallization, leading to a dehydrated phase **4**. The crystal structure remains monoclinic $P2_1/c$ during the phase transition, with the *c*-axis elongating.

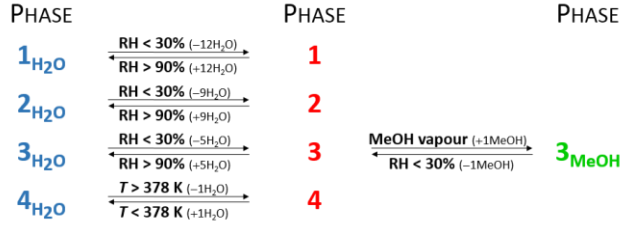

Scheme 2. Crystal transformations in complex salts with DABCO- and ABCO-based cations and bis(oxalato)chromium(III) anions.

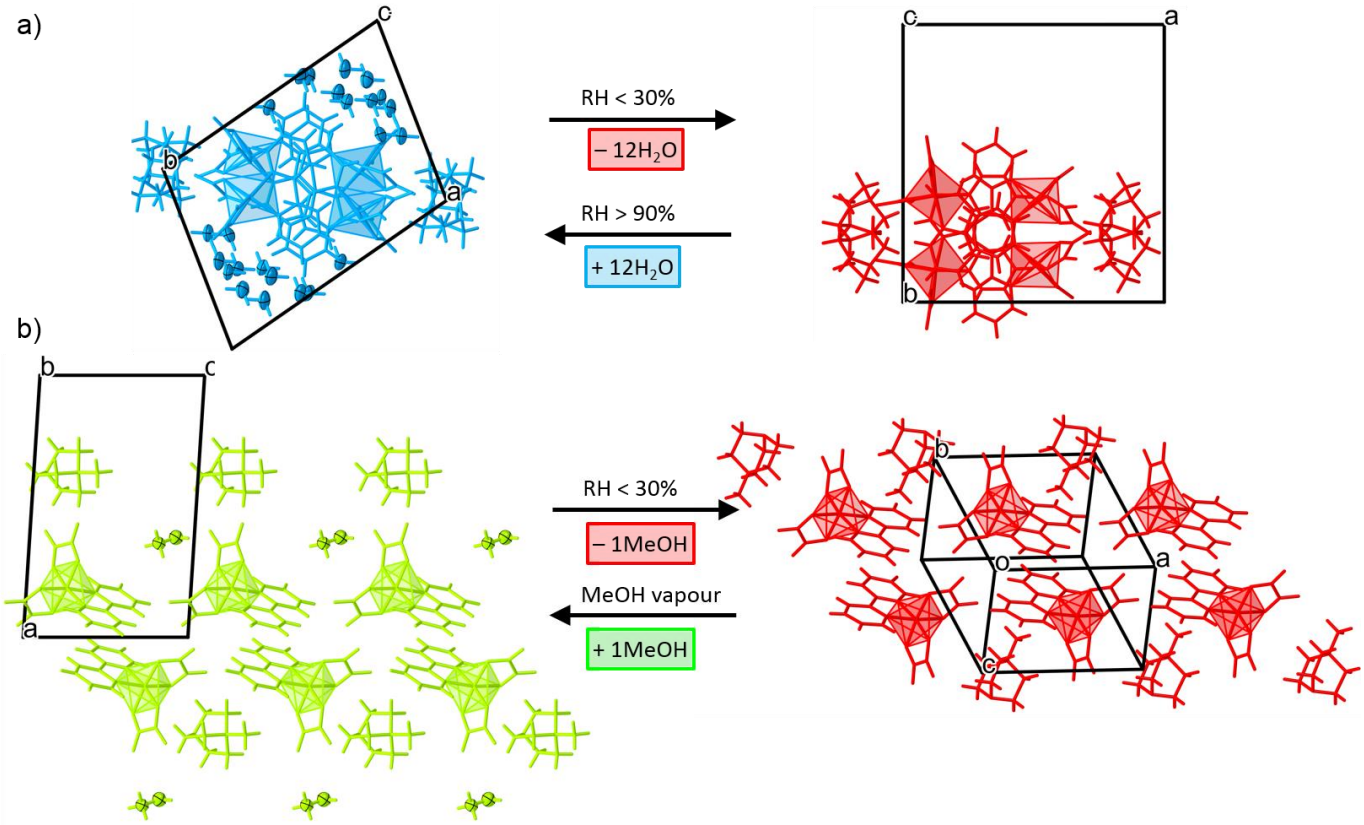

Figure 5. Change in the crystal packing during the reversible transformation of hydrated form $\mathbf{1}_{H_2O}$ to dehydrated form **1** (a), and compound $\mathbf{3}_{MeOH}$ to desolvated form **3** driven by exposure to dry air or methanol vapour (b).

Below 378 K the structure returns to the initial room temperature phase and the water molecule of crystallization is being reabsorbed from the air.

Thermal stability

In order to determine the thermal stability of compounds **1**, **2**, and $\mathbf{3}_{H_2O}$–$\mathbf{6}_{H_2O}$, simultaneous TG and DTA analyses were carried out in a stream of synthetic air. We were unable to collect the TG/DTA data of the hydrated phases $\mathbf{1}_{H_2O}$ and $\mathbf{2}_{H_2O}$ due to rapid crystal transformations that occur when these compounds are removed from the humid atmosphere. The character of thermal decomposition for all compounds is very similar (full range TG and DTA curves are given in Figure S16, ESI†). Compounds $\mathbf{4}_{H_2O}$–$\mathbf{6}_{H_2O}$ are more stable than $\mathbf{3}_{H_2O}$, losing their crystallization water molecules above 373 K which is evident from the TG curves presented in Figure S16, accompanied by a broad DTA minimum in the temperature range of 400–500 K. In all compounds organic cations and bis(oxalato)chromium(III) anions start to decompose above 473 K. The degradation is finished by an extremely exothermic process – the DTA curve shows an intensive maximum around 650 K. Afterwards, the remaining mass stays constant and corresponds to chromium(III) oxide.

Dielectric and conductivity study

The frequency-dependent and iso-frequency dielectric permittivity (ε' and ε'') studies were performed on desolvated phase **1** and compounds $\mathbf{3}_{MeOH}$ and $\mathbf{4}_{H_2O}$–$\mathbf{6}_{H_2O}$ with varying temperatures from 183 K to 363–423 K, dependent on the thermal stability of the compound (Figure S16). Figure 6 shows the temperature dependence of the dielectric constant, ε', measured at 100 kHz and the corresponding dielectric loss, $\varepsilon''/\varepsilon'$, is given in ESI together with the data collected at 10 kHz (Figures S17–S19). Dielectric constant value for dehydrated compound **1** changes only slightly with temperature variations, from 15.3 to 16.0, with a distinct peak around 250 K indicative of the thermally activated molecular motion of the $(H_2\text{-DABCO})^{2+}$ cation.[44] Compound $\mathbf{5}_{H_2O}$ also has a peak in the dielectric loss around 250 K (Fig. S14c) suggesting dissipation of the electric energy due to the dynamics of polar $[H\text{-(COOH)(OH)ABCO}]^{+}$ cations (dielectric relaxation). Compound $\mathbf{3}_{MeOH}$ shows three different behaviours during the temperature increase. Below 233 K the dielectric constant shows a low value ($\varepsilon' \approx 10$), which is almost independent of temperature and frequency. Meanwhile, at >233 K ε' increases markedly with

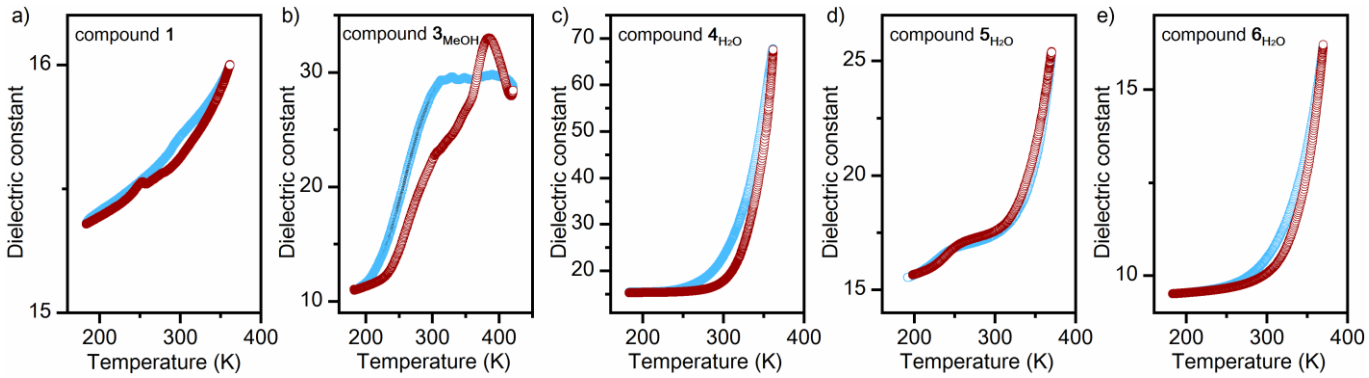

Figure 6. Temperature dependence of dielectric constant (ε') during heating (dark red) and cooling (blue) for compounds **1**, $\mathbf{3_{MeOH}}$, $\mathbf{4_{H_2O}}$, $\mathbf{5_{H_2O}}$, and $\mathbf{6_{H_2O}}$ measured at 100 kHz.

temperature reaching a value of $\varepsilon' = 22$ at room temperature. Another interesting feature is the well-resolved peak that is observed around 383 K. Anomalies that are observed in the dielectric constant of compound $\mathbf{3_{MeOH}}$ together with the high dielectric loss measured in both heating and cooling runs could be related to the reversible structural transformations involving desolvation/resolvation process.[45]

In compounds $\mathbf{4_{H_2O}}$ and $\mathbf{6_{H_2O}}$ the dielectric constant and loss gradually increase while increasing the temperature and decrease toward higher frequencies (Figure S20, ESI). There is a good overlap between heating and cooling runs. The conductivity of compound $\mathbf{4_{H_2O}}$ increases four orders of magnitude by the increase in temperature, from $1.05 \cdot 10^{-10}$ S cm^{-1} at 230 K to $2.98 \cdot 10^{-6}$ S cm^{-1} at 361 K. The observed increase in dielectric constant is related with the reversible phase transition that compound $\mathbf{4_{H_2O}}$ undergoes at 378 K. Such materials that show switchable dielectric transitions between high- and low- dielectric states during the phase transition are of great interest in the field of electrical and electronic devices.[13,46,47]

Humidity sensing properties of compounds 1–3

Humidity sensing experiments were performed on a pressed pellet of dehydrated forms **1**–**3**, by alternately passing dry and water-saturated air at room temperature. The current response to changes in relative humidity is presented in Figure 7 for compounds **1**–**3**. As can be seen, compound **1** shows reversible electrical changes with changes in humidity. At low humidity (below 30% RH) the current response is in the nA range (below 10 nA). Spectroscopic and diffraction studies of the dry phase of **1** show that it does not contain solvent molecules (Figures S3 and S7). At very high humidity (above 90% RH) there is a striking increase in the current, reaching the µA range (by three orders of magnitude). This is associated with the formation of a new phase, $\mathbf{1_{H_2O}}$, which contains 12 crystallization water molecules as detected by spectroscopic and diffraction methods (Figures S3 and S8). The apparent hysteresis that exists between the drying and wetting processes is probably due to the gradual release of water molecules from the structure at room temperature and pressure. This is in good agreement with time dependent ATR measurements (Figure S14), which also show that water molecules are being released from the structure of $\mathbf{1_{H_2O}}$ gradually. The total change in current response between the dry form **1** and wet form $\mathbf{1_{H_2O}}$ is by a factor of 1500. Reproducibility between cycles of drying/wetting is very good, and multiple cycles can be performed on a single pressed pellet. Even after more than a month of storage at room temperature in air, we found that the performance of the last measurement attempt was indistinguishable from that of the first, indicating the high reliability. A similar dehydration/rehydration behaviour was observed for compound **2**, which was accompanied by a structural transition and a change in the current response to relative humidity. The formation of the hydrated phases $\mathbf{1_{H_2O}}$ and $\mathbf{2_{H_2O}}$ supports water-mediated proton conductivity and the overall increase in conductivity under humid conditions is observed. This is in correlation with the crystal structure of hydrated forms, where water molecules of crystallization surround the $(H_2\text{-DABCO})^{2+}$ cations forming an extended hydrogen bond network, that serves as a proton transport pathway.[46]

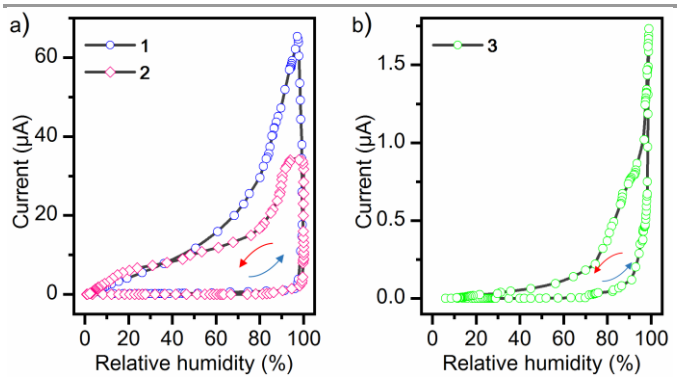

Figure 7. Change in the current response (conductivity) upon increases and decreases in the relative humidity of compound **1** and **2** (a) and **3** (b).

In order to elucidate the mechanism of humidity sensing for **3**, we have performed the sensing experiments on a single-crystal. These experiments have shown that crystal structure of **3** indeed exhibits a breathable behaviour and that the structural changes during the water entrapment are not damaging to the crystal. This is an indication that humidity sensing in compound **3** is accompanied by a single-to-single-crystal transformation. Furthermore, compound **3** can be converted to the initially obtained methanol solvate structure, $\mathbf{3_{MeOH}}$, when exposed to methanol vapour. The hysteresis between wetting and drying in compound **3** is smaller than for compounds **1** and **2**, probably due to the lower uptake of crystallization water molecules. Nevertheless, the relative changes in the current response of more than 1000 are remarkable, clearly indicating that the studied compounds have promising properties as sensing materials.

Thermistor properties of compound 4

To investigate the thermistor performance of compound $\mathbf{4_{H2O}}$, we used chronoamperometry in a two-electrode configuration. Tests were performed on a single-crystal of $\mathbf{4_{H2O}}$ attached to gold wires with a silver adhesive. Heating was done with a heat gun and reached a maximum temperature of about 358 K. We found that the current increased sharply with increasing temperature (Figure 8). When the crystal was allowed to cool to room temperature, the current output reached the initial value. These observations are consistent with the impedance measurements shown in Figure 6c. The response/recovery process is very fast. The origin of a sudden increase in conductivity of $\mathbf{4_{H2O}}$ is related to the movement of $[H\text{-}(O)ABCO]^+$ cations and to the release of one water molecule in the crystal structure. In the room temperature phase, the $[H\text{-}(O)ABCO]^+$ cations form very strong hydrogen bonds with the oxalate groups of the $[Cr(bpy)(C_2O_4)_2]^-$ anions, preventing the rotational dynamics of the cation. After the phase transition at 378 K, the $[H\text{-}(O)ABCO]^+$ cations have more rotational freedom, and in the crystal structure we observe that the oxo-oxygen atom is disordered in two positions with half occupancies. The rotational angle of $[H\text{-}(O)ABCO]^+$ cations is 122°, which is the typical vale of rotation for molecules of the azabicyclo[2.2.2]octane family.[48]

In the high-temperature phase, the $[H\text{-}(O)ABCO]^+$ cations occupy positions that allow short contacts between neighbouring molecules (yellow dash line in Figure 8b). The overall motion of the $[H\text{-}(O)ABCO]^+$ cations serves in process of formation of continuous conducting pathways for ionic conduction in compound **4** above 378 K. This type of conductivity in solids is of fundamental interest due to potential applications in energy storage, conversion devices and chemical sensors.[49]

These results are comparable to the recently published stimuli-responsive electrically bistable materials, where switchable conductivity states with an ON/OFF current ratio of 10^5 was observed in a co-crystal of 1,3,5-triazine-2,4,6-triamine, melamine and pyrazine-2,3-dicarboxylate.[50] Thermally triggered dielectric switching was also observed in host-guest cyanometallate $(MA)(H_2O)[Sr(H_2O)_2Co(CN)_6]$ (MA = methylammonium) metal-organic framework, but with a considerably lower switching ratio between the high and low dielectric state.[16] Dielectric switching ratios for metal-organic hybrid systems are typically smaller than 10,[15,46,47,51,52] excluding molecular ferroelectric where these ratios can reach higher values.[7,14,15]

Conclusions

Herein, we report the mechanochemical synthesis of six new bis(oxalato)chromium(III) complex salts with derivatives of 1,4-diazabicyclo[2.2.2]octane (DABCO) and 1-azabicyclo[2.2.2]octane (ABCO) cations. Structural and spectroscopic measurements have shown that compounds **1–3** with derivatives of DABCO cations and bis(oxalato)chromium(III) anions undergo reversible single-crystal-to-single-crystal transformations associated with desolvation/resolvation processes triggered by a change in the humidity of the surrounding atmosphere. Removal of crystallization water molecules from hydrated forms $\mathbf{1_{H2O}}$, $\mathbf{2_{H2O}}$, and $\mathbf{3_{H2O}}$ in dry atmosphere (RH < 30%) leads to a significant decrease in the conductivity of dehydrated forms **1**, **2**, and **3**. Moreover, we showed that compound **3** is reversibly transformed into compound $\mathbf{3_{MeOH}}$ when exposed to methanol vapour. Desolvation/resolvation processes and associated

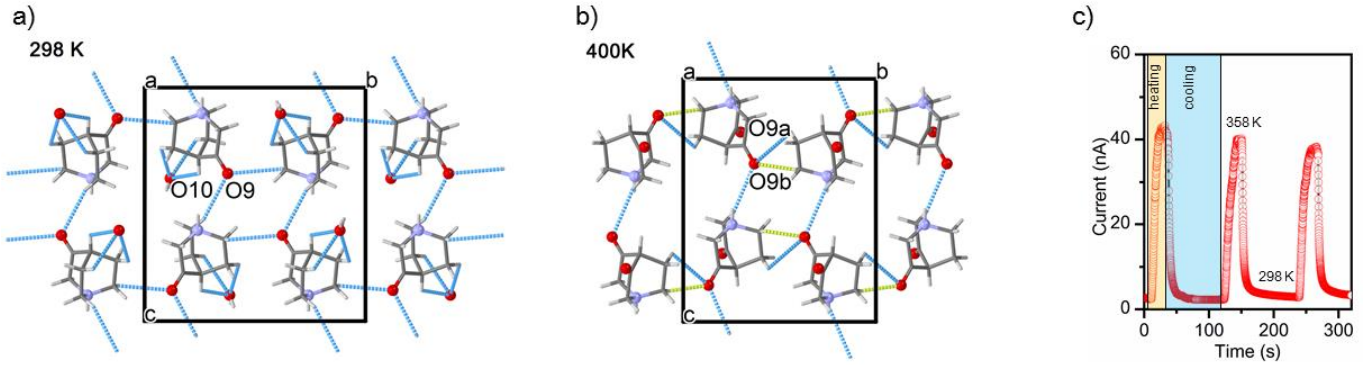

Figure 8. Hydrogen bonding between $[H\text{-}(O)ABCO]^+$ cations in compound $\mathbf{4_{H2O}}$ at room temperature (a) and dehydrated form **4** at 400 K (b). Current response for compound $\mathbf{4_{H2O}}$ at 10 V during heating with heat gun at 358 K and cooling to 298 K (c).

electrical responses to structural transformations in these systems may be of interest for the development of advanced gas sensing technologies, for applications such as breath analysis or air quality monitoring. The phase transition in compound $\mathbf{4}_{\mathbf{H_2O}}$ which occurs at 378 K also affects the electrical properties of the material. The excellent thermistor sensitivity of compound $\mathbf{4}_{\mathbf{H_2O}}$ can be attributed to the dynamic movement of the $[H\text{-}(O)ABCO]^+$ cation with increasing temperature. Overall, complex salts of DABCO- and ABCO-based cations and bis(oxalato)chromium(III) anions, prepared by a simple and environmentally friendly mechanochemical approach, have been shown to exhibit exceptional structural, optical (pleochroic) and electrical properties, and due to these features represent promising materials for application in (humidity, alcohol, temperature) sensing devices. Our further research will be related to the use of the respective complex salts in different device architectures and the exploration of their new functionalities, such as capture of different molecules (*e.g.* NH_3, SO_2, CO_2, CO, CH_4).

Conflicts of interest

There are no conflicts to declare.

Acknowledgements

Financial support from the Croatian Science Foundation (UIP-2019-04-7433) is gratefully acknowledged.

Notes and references

1 C. Tianliang, Z. Yuelan, S. Zhihua, Z. Shuquan, Z. Sangen, T. Yuanyuan, J. Chengmin and L. Junhua, *Inorg. Chem.,* 2015, **54** (15), 7136–7138.

2 Y. Liu, C.-l. Zhu, X.-y. Zheng, L.-l. Qin, S.-x. Yang and Z.-q. Liu, *R. Soc. open sci.*, 2018, **5**, 180738.

3 Y. Yu, M. Nakano and T. Ikeda, *Nature*, 2003, **425**, 145.

4 M. Wuttig and N. Yamada, *Nat. Mater*. 2007, **6**, 824–832.

5 M. Samoc, N. Gauthier, M. P. Cifuentes, F. Paul, C. Lapinte and G. Humphrey, *Angew. Chem., Int. Ed.*, 2006, **45**, 7376–7379.

6 L. K. Ono, E. J. Juarez-Perez and Y. Qi, *ACS Appl. Mater. Interfaces* 2017, **9**, 30197–30246.

7 J. Harada, T. Shimojo, H. Oyamaguchi, H. Hasegawa, Y. Takahashi, K. Satomi,Y. Suzuki, J. Kawamata and T. Inabe, *Nat. Chem.,* 2016, **8** (10), 946–952.

8 Y.-Y. Tang, P.-F. Li, W.-Y. Zhang, H.-Y. Ye, Y.-M. You and R.-G. Xiong, *J. Am. Chem. Soc.*, 2017, **139** (39), 13903–13908.

9 W.-Y. Zhang, Y.-Y. Tang, P.-F. Li, P.-P. Shi, W.-Q. Liao, D.-W. Fu, H.-Y. Ye, Y. Zhang and R.-G. Xiong, *J. Am. Chem. Soc.,* 2017 **139** (31), 10897–10902.

10 J.-C. Liu, W.-Q. Liao, P.-F. Li, Y.-Y. Tang, X.-G. Chen, X.-J. Song, H.-Y. Zhang, Y. Zhang, Y.-M. You and R.-G. Xiong, *Angew. Chem. Int. Ed.*, 2020, **59** (9), 3495–3499.

11 P. González-Izquierdo, O. Fabelo, L. Cañadillas-Delgado, G. Beobide, O. Vallcorba, J. Salgado-Beceiro, M. Sánchez-Andújar, C. Martin, J. Ruiz-Fuentes, J. E. García, M. T. Fernández-Díaz and I. de Pedro*, J. Mater. Chem. C*, 2021, **9**, 4453–4465.

12 J.-Y. Li, Q.-L. Xu, S.-Y. Ye, L. Tong, X. Chena and L.-Z. Chen, *Chem. Commun*., 2021, **57**, 943–946.

13 K. Pasińska, A. Ciupa, A. Pikul, A. Gągor, A. Pietraszko and A. Ciżman, *J. Mater. Chem. C*, 2020, **8**, 6254–6263.

14 K. Pasińska, A. Piecha-Bisiorek, V. Kinzhybalo, A. Ciżman, A. Gągor and A. Pietraszko, *Dalton Trans.*, 2018, **47**, 11308–11312.

15 T. Zhang, C. Chen, W.-Y. Zhang, Q. Ye and D.-W. Fu, *Inorg. Chem. Front.*, 2018, 5, 2340–2345.

16 Y.-L. Liu and W. Zhang, *Chem. Comm*., 2017, **53**, 6077–6080.

17 G. Marinescu, M. Andruh, F. Lloret and M. Julve, *Coord. Chem. Rev*., 2011, **255**, 161–185.

18 F. D. Rochon, R. Melanson and M. Andruh, *Inorg. Chem.*, 1996, **35**, 6086–6092.

19 G. Marinescu, M. Andruh, M. Julve, F. Lloret, R. Llusar, S. Uriel and J. Vaissermann, *Crystal Growth & Design,* 2005, **5**, 261–267.

20 M. Andruh, R. Melanson, C.V. Stager and F.D. Rochon, *Inorg. Chim. Acta*,1996, **251**, 309–317.

21 L. Androš, M. Jurić, K. Molčanov and P. Planinić, *Dalton Trans.*, 2012, **41**, 14611–14624.

22 L. Androš Dubraja, M. Jurić, F. Torić and D. Pajić, *Dalton Trans.*, 2017,**46**, 11748–11756.

23 L. Androš Dubraja, M. Jurić, J. Popović, D. Pajić, Y. Krupskaya, V. Kataev, B. Bűchner and D. Žilić, *Dalton Trans.*, 2018, **47**, 3992–4000.

24 E. Coronado, J. R. Galan-Mascaros and C. Martí-Gastaldo, *J. Am. Chem. Soc.* 2008, **130**, 14987–14989.

25 D. Hirai, T. Yajima, D. Nishio-Hamane, C. Kim, H. Akiyama, M. Kawamura, T. Misawa, N. Abe, T Arima and Z. Hiroi, *J. Am. Chem. Soc.*,2017 **139**, 10784–10789.

26 J.-Y. Kazock, M. Taggougui, B. Carré, P. Willmann and D. Lemordant, *Synthesis*, 2007, **24**, 3776–3778.

27 C. A. Grob and E. Renk, *Helvetica*, 1954, 37, 1689–1698.

28 Agilent, CrysAlis PRO, Agilent Technologies Ltd, Yarnton, Oxfordshire, England, 2014.

29 M. C. Burla, R. Caliandro, B. Carrozzini, G. L. Cascarano, C. Cuocci, C. Giacovazzo, M. Mallamo, A. Mazzone and G. Polidori, *J. Appl. Cryst.*, 2015, **48**, 306–309.

30 G. M. Sheldrick, *Acta Cryst. C,* 2015, **71**, 3–8.

31 L. J. Farrugia, *J. Appl. Cryst.*, 2012, **45**, 849–854.

32 L. Spek, *Acta Cryst. D*, 2009, **65**, 148–155.

33 F. Macrae, P. R. Edgington, P. McCabe, E. Pidcock, G. P. Shields, R. Taylor, M. Towler and J. van de Streek, *J. Appl. Cryst*., 2006, **39**, 453–457.

34 TOPAS version 4.2, Bruker-AXS, Karlsruhe, Germany.

35 G. S. Pawley, *J. Appl. Crystallogr*., 1981, **14**, 357–361.

36 K. Maity, D. Mukherjee, M. Sen, and K. Biradha, *ACS Appl. Nano Mater.*, 2019, **2**, 1614−1620.

37 J. Vainauskas, F. Topić, O. S. Bushuyev, C. J. Barrett and T. Friščić, *Chem. Comm.*, 2020, **56**, 15145–15148.

38 A. B. P. Lever, *Inorganic Electronic Spectroscopy*, Elsevier, Amsterdam, 1968

39 K. Nakamoto, *Infrared and Raman Spectra of Inorganic and Coordination Compounds*, John Wiley, New York, 6th edn, 2009.

40 Y. Xin, J. Wang, M. Zychowicz, J. J. Zakrzewski, K. Nakabayashi, B. Sieklucka, S. Chorazy and S Ohkoshi, *J. Am. Chem. Soc.*, 2019, **141**, 18211–18220.
41 L. Chen, J.-W. Ye, H.-P. Wang, M. Pan, S.-Y. Yin, Z.-W. Wei, L.-Y. Zhang, K. Wu, Y.-N. Fan and C.-Y. Su, *Nature Comm.*, 2018, **8**, 15985.
42 S. Nakatsuka,Y. Watanabe, Y. Kamakura, S. Horike, D. Tanaka and T. Hatakeyama*, Angew. Chem. Int. Ed.*, 2020, **59**, 1435–1439.
43 Y.-P. Lin, L.-C. Rao, M.-J. Zhao, X.-Y. Huang, and K.-Z. Du, *Dalton Trans.*, 2021, **50**, 2001–2006.
44 T. Sakurai, R. Saiki, R. Jia Wei, G. N. Newton, T. Shiga and H. Oshio, *Dalton Trans*., 2016, **45**, 16182–16189.
45 M. Sánchez-Andújar, S. Yáñez-Vilar, B. Pato-Doldán, C. Gómez-Aguirre, S. Castro-García and M. A. Señarís-Rodríguez, *J. Phys. Chem. C*, 2012, **116**, 13026–13032.
46 A. Cizman, D. Kowalska, M. Trzebiatowska, W. Medycki, M. Krupiński, P. Staniorowski and R. Poprawski, *Dalton Trans.*, 2020, **49**, 10394–10401.
47 L. Ye, Z.-X. Gong, C. Shi, J.-J. Ma, H. Liang, F.-W. Qi, D.-Y. E, C.-F. Wang, Y. Zhang and H.-Y. Ye, *CrystEngComm*, 2019, **21**, 7043–7047.
48 A. Navarro-Huerta, M. J. Jellen, J. Arcudia, S. J. Teat, R. A. Toscano, G. Merino and B. R. Molina, *Chem. Sci.*, 2021, **12**, 2181–2188.
49 H.-N. Wang, X. Meng, L.-Z. Dong, Y. Chen, S.-L. Li and Y.-Q. Lan, *J. Mater. Chem. A*, 2019, **7**, 24059–24091.
50 Q. Liu, L. Zhao, W. Wu, Y. He, K. Song, J. Qi, H. Li and Z. Chen, *J. Mater. Chem. C*, 2020, **8**, 3258–3267.
51 C. Shi,X. Zhang,Y. Cai, Y.-F. Yao and W. Zhang, *Angew. Chem., Int. Ed.*, 2015, **54**, 6206–6210.
52 A. Zeb, Z. Sun, A. Khan, S. Zhang, T. Khan, M. A. Asghar and J. Luo, *Inorg. Chem. Front.*, 2018, 5, 897–902.